Pis'ma v ZhETF, vol. 100, iss. 7, pp. 484 – 488

Optical Tamm states in arrays of all-dielectric nanoparticles

R. S. Savelev[+1)], *A. E. Miroshnichenko*[*], *A. A. Sukhorukov*[*], *Y. S. Kivshar*[+*]

[+]*ITMO University, 197101 St. Petersburg, Russia*

[*]*Nonlinear Physics Center, Research School of Physics and Engineering, Australian National University, Canberra, ACT 0200, Australia*

Submitted 7 July 2014

We predict that edges of a finite one-dimensional array of high-index dielectric nanoparticles can support evanescent optical modes localized near the edge, which represent an optical analogue of the well-known electronic Tamm states in solids. We describe the properties of such modes for different types of the edge defect by employing dipole-dipole approximation.

DOI: 10.7868/S0370274X14190035

Interfaces separating different physical media can support a special class of transversally localized modes known as surface waves. Linear surface waves have been studied extensively in many branches of physics [1]. As was first predicted by I.E. Tamm [2], a special type of localized electronic states can exist at the edge of a truncated periodic potential, and this study opened the field of surface physics of solids in the 1930s. Such Tamm states are associated with the presence of a certain type of surface defect, and they were found in other systems, e.g., at an interface separating periodic and homogeneous dielectric optical media including surface phonons [3] and surface polaritons [4].

Electromagnetic surface waves are known to exist as the waves localized at the interface separating either two homogeneous or homogeneous and periodic dielectric media [5]. It was also shown that arrays of weakly coupled optical waveguides can support different types of linear and nonlinear states localized at and near the waveguide edge (see, e.g. [6] and references therein). It was found that Tamm surface waves can exists at the edge of an array of optical waveguides when the value of the effective refractive index of the boundary waveguide is above a certain threshold [7].

Recently, a novel type of subwavelength guiding of light has been demonstrated with arrays of spherical dielectric nanoparticles with high values of the optical refractive index [8, 9]. Dielectric nanoparticles support both magnetic dipole (MD) and electric dipole (ED) resonances simultaneously [10, 11]. This gives an additional control parameter over the light scattering [12], and the waveguides composed of such nanoparticles were shown to support several modes of different types [9]. Defects in such structures can easily appear during the fabrication process, or otherwise implemented artificially. This could lead to the presence of modes localized near the defects.

In this Letter we study localized edge states in a chain of spherical dielectric particles, which are formed by introducing a defect at the edge of the chain. We consider a chain of $N = 20$ particles with the period of the chain $a = 200$ nm, radius of the spheres $r = 70$ nm and permittivity $\varepsilon_p = 16$, which corresponds to silicon in optical frequency range. Two types of defects are considered: different radius R of the leftmost particle, and different separation distance $a_{\rm def} = a - L$ between the two leftmost particles (see Fig. 1). In our calculations,

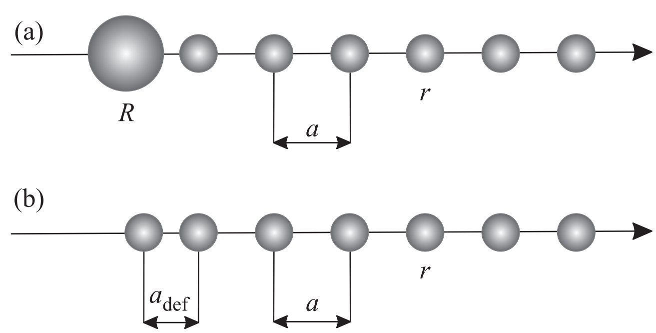

Fig. 1. Schematic of chains of dielectric spheres of radius r and period a with two types of defect: different radius of the leftmost sphere R (a), different distance between two leftmost spheres $a_{\rm def} = a - L$ (b)

we do not take into account the material dispersion of silicon because the real part of the permittivity does not change significantly in the required spectral range, and the imaginary part can be ignored for dielectric materials [13].

[1)]e-mail: r.saveliev@phoi.ifmo.ru

It was shown that modes of an infinite chain of high-refractive index dielectric particles can be described with a good accuracy by the coupled-dipole approximation [9], i.e. when particles are treated as hybrid MD and ED with magnetic and electric momenta, oscillating with frequency ω [$\propto \exp(-i\omega t)$] [14, 15]. Due to the fact that a magnetic dipole mode describes the fundamental response of a high-dielectric spherical particle and all other multipoles are suppressed (see, for example Supplementary Information in Ref. [10]), this model gives very accurate results in the vicinity of the magnetic dipole resonance, especially in the case of longitudinal polarization, i.e. when MDs are oriented along the chain, and EDs are not excited. Therefore we simplify our analysis by considering the case of longitudinally polarized magnetic modes. Then a finite chain without defects can be described by a set of coupled equations for N magnetic moments in the following form [16]:

$$\mathbf{Cm} = 0,$$

where $\mathbf{m}$ is the column-vector of magnetic moments oriented along the chain axis of the length N, and $\mathbf{C}$ is the $N \times N$ matrix of interaction coefficients:

$$C_{ij} = \frac{1}{\alpha_m(\omega)},\ i = j,$$

$$C_{ij} = -\frac{2\exp(ik_h d_{ij})}{d_{ij}^2}\left(\frac{1}{d_{ij}} - ik_h\right),\ i \neq j,$$

where $\alpha_m = 3ib_1^{sc}/2k_h^3$ is the magnetic polarizability of the sphere with b_1^{sc} being the scattering coefficient that depends on permittivity and radius of the sphere [17], $d_{ij} = a|i-j|$ is the distance between the centers of i-th and j-th spheres, ε_h is the permittivity of the host medium, and $k_h = \sqrt{\varepsilon_h}\omega/c$ is the host medium wavenumber. When we introduce a size defect to the leftmost particle, we assign $C_{11} = 1/\alpha_m^{\mathrm{def}}$, where α_m^{def} is the magnetic polarizability of the defect sphere. And for the interparticle distance defect: $d_{kl} = a|k-l| + L$ when $k = 1$ or $l = 1$.

Eigenfrequencies of the considered system are defined as zeros of the function:

$$F(\omega) = \det[\mathbf{C}]. \tag{1}$$

In Fig. 2a we show a complex plane $[\mathrm{Re}(\omega), \mathrm{Im}(\omega)]$ with thick black curves corresponding to the solutions of the equation $\mathrm{Re}[F(\omega)] = 0$ and blue thick curves corresponding to the solutions of the equation $\mathrm{Im}[F(\omega)] = 0$, for a chain with a size defect sphere of radius $R = 75$ nm. Twenty solid red circles show the eigenfrequencies corresponding to Fabry-Pérot resonances in a chain without

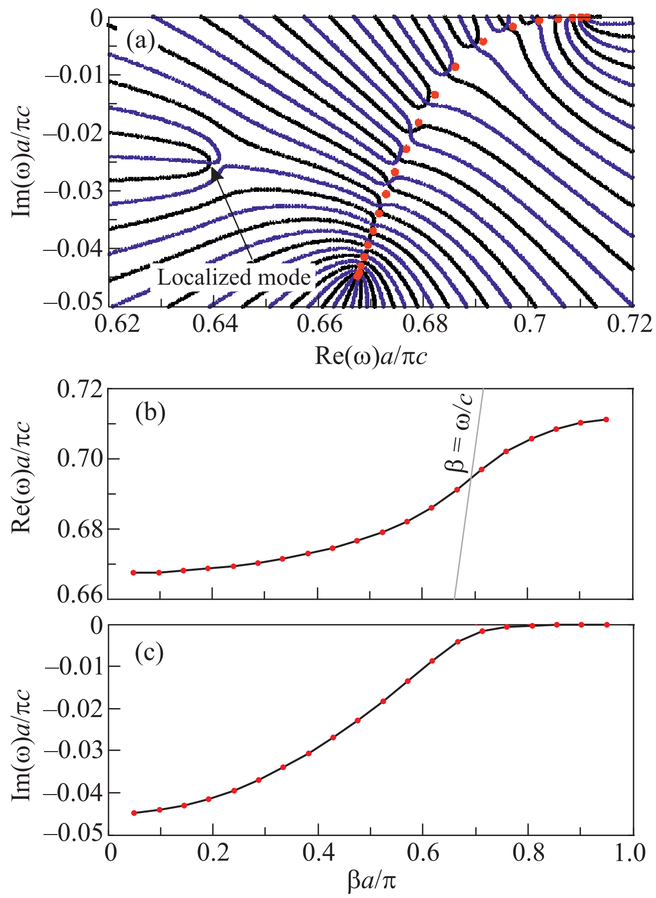

Fig. 2. (Color online) (a) – Complex plane $[\mathrm{Re}(\omega), \mathrm{Im}(\omega)]$ with thick black curves corresponding to the solutions of the equation $\mathrm{Re}[F(\omega)] = 0$ and blue thick curves corresponding to the solutions of the equation $\mathrm{Im}[F(\omega)] = 0$, for a chain with a defect sphere of radius $R = 75$ nm; solid red circles show the eigenfrequencies of a chain without defect. (b, c) – Dispersion diagram of a chain without defect; $\beta a/\pi$ is a normalized Bloch wavenumber

defect, which form a passband of considered periodic structure. Corresponding eigenmodes can be interpreted as Bloch waves with wavenumbers being defined from the mode profiles [16]. Dispersion diagram for this structure is shown in Figs. 2b and c. Due to radiative losses all eigenfrequencies are complex. Passband is observed in the spectral region $0.667 \lesssim \mathrm{Re}(\omega)a/\pi c \lesssim 0.712$. Modes that lie below the light line (i.e. with $\beta > \mathrm{Re}(\omega)/c$) are characterized by low radiative losses with small imaginary parts of ω, and can be considered as subradiant modes. Other modes lie above the light line and thus are characterized by fast radiative damping with large values of $\mathrm{Im}(\omega)$, and can be considered as superradiant modes.

When we introduce a defect in the finite chain, $N-1$ eigenmodes stay in the passband with both real and imaginary parts of eigenfrequencies approximately the same as in ideal periodic structure; which means that the guiding properties of this chain are not significantly affected by the presence of a defect in the structure. At the same time, one eigenfrequency that corresponds to the defect mode lies outside the passband (see Fig. 2a). Thus, the defect mode corresponds to an evanescent wave and becomes localized near the edge of the truncated chain. Eigenfrequency of this localized defect mode as a function of the difference between the radius of the defect and other spheres $R-r$ is plotted in Fig. 3. For $R>r$, i.e. when MD resonance frequency

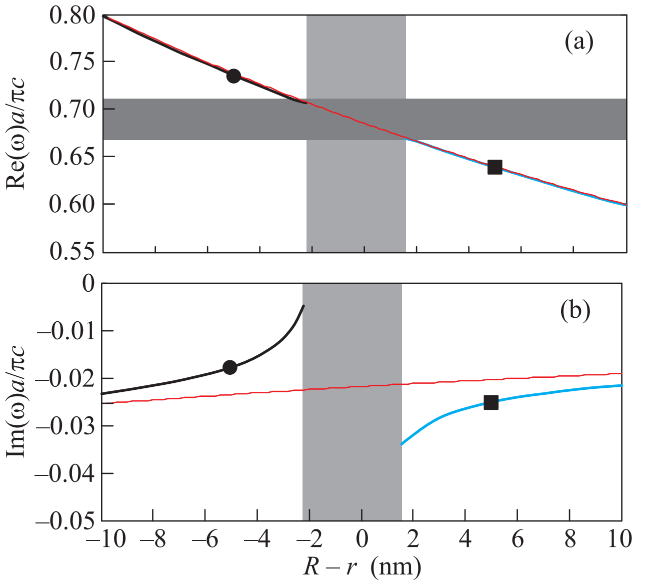

Fig. 3. (Color online) Black and blue lines show real (a) and imaginary (b) parts of the normalized eigenfrequency of the defect mode as a function of the difference between the radii of defect sphere R and other spheres r. Red solid line corresponds to the complex resonance frequency of a single sphere of radius R. Dark grey area in Fig. a shows the passband of the structure without defect. Vertical light grey areas in Figs. a and b indicate the values of $R-r$ at which the defect mode does not exist

of the defect sphere is lower than that of other spheres, defect eigenmode becomes *superradiant defect mode*. In the opposite case for $R<r$, when the eigenfrequency of the defect mode lies above the passband, we observe the formation of *subradiant defect mode*. Such description can also be justified by their corresponding imaginary parts (see Fig. 3b).

Defect modes profiles for $R=80$ and $R=60$ nm are shown in Figs. 4a and b, respectively. Mode with lower frequency emerges from the lower edge of the Brillouin zone when R is about 72 nm. At this point all dipoles oscillate in phase, and this mode is strongly radiative (imaginary part of eigenfrequency is large). When the radius of the defect sphere increases, dipoles tend to dephase and radiative damping rate of this mode decreases (see Fig. 3b). A mode with higher frequency emerges from the upper edge of the Brillouin zone (with $\beta=\pi/a$) when R is about 68 nm. At this point the neighbouring dipoles oscillate out-of-phase, i.e. this mode is staggered, and it has low radiative damping rate due to interference of the dipoles radiation. Similarly, when R becomes smaller, out-of-phase configuration starts to break, and an imaginary part of eigenfrequency grows (see Fig. 3b) – this mode radiates faster.

In Fig. 3 we also show the complex eigenfrequency of a single sphere with radius R by thin red line. We observe that the real part of the defect mode eigenfrequency is practically the same as that of a single sphere with radius R. However imaginary part is quite different for small values of $|R-r|$, when there remains rather strong interaction between the defect sphere and other spheres. Ultimately, for large values of $|R-r|$ when MD resonance frequencies of the spheres with radii R and r substantially differ, interaction becomes very weak. Consequently, there exist $N-1$ modes of a chain of $N-1$ spheres of radius r, and one mode which is a MD resonance of a single sphere with radius R.

For spacing type of defect, the eigenfrequencies of defect modes as a function of defect parameter $L=a-a_{\mathrm{def}}$ are shown in Fig. 5. In this case, when we reduce the distance between the two leftmost spheres by ≈ 30 nm, two defect modes emerge above and below the passband as indicated by black and blue curves in Fig. 5. Since in this case all spheres are of the same radius, both real and imaginary parts of the defect modes weakly depend on the value of L, still maintaining their super- and subradiant character (see Fig. 5b).

In conclusion, we have studied a novel type of optical states localized at the edge of a truncated array of high-index dielectric nanoparticles, which represents an optical analogue of the well-known electronic Tamm states in solids. We have employed the dipole approximation, which is known to be well suited for theoretical study of electromagnetic properties of such structures. We have analyzed the properties of the optical localized modes for different types of the edge defects. We have shown that when the edge sphere has a different radius R, localized mode is observed at the frequency that corresponds to the resonance of a single sphere with radius R, when $|R-r|$ is larger than a certain critical value of about 2 nm. Furthermore, for small values of $|R-r|$ ($\lesssim 10$ nm), localized modes exhibit super- or sub-radiant properties compared to those of a single dipole. This

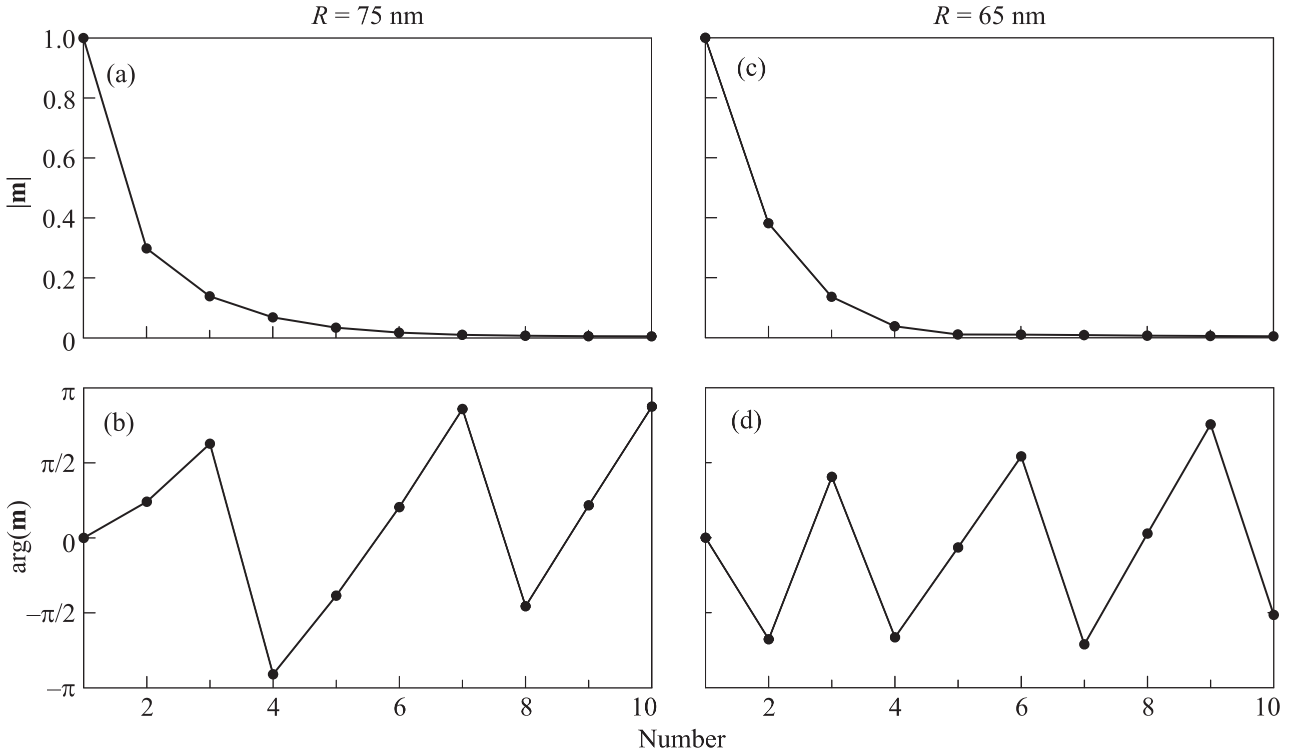

Fig. 4. Amplitude (a, c) and phase (b, d) of magnetic moments distribution in the defect modes of a chain with defect sphere of radius $R = 75$ nm (a, b) and 65 nm (c, d), indicated by black circle and square in Fig. 3, respectively

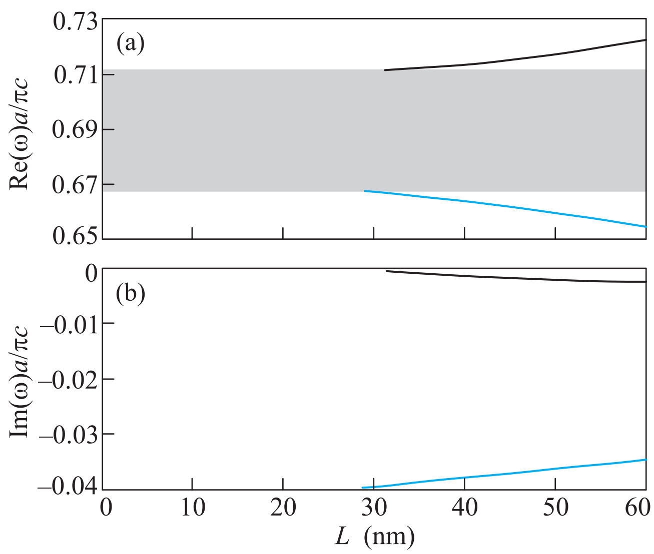

Fig. 5. (Color online) Real (a) and imaginary (b) parts of the normalized eigenfrequency of the defect mode as a function of the spacing defect parameter L. Grey area in Fig. a shows the pass band of the structure without defect

can be explained by the interaction between the defect and rest of the chain. When a defect is introduced by varying the distance between the two edge particles, we observe simultaneously both super- and sub-radiant localized modes emerging above and below the passband at a certain value of the defect parameter L. An important difference in this case is that the radiation damping rate of these modes depends weakly on the separation distance L.

This work was supported by the Ministry of Education and Science of the Russian Federation (GOSZADANIE 2014/190), the Government of Russian Federation (Grant # 074-U01), by RFBR Project # 14-02-31761, the Dynasty Foundation (Russia), and the Australian Research Council (ARC) via the Future Fellowship and Discovery Project programs. Study of defect modes was supported by the Russian science foundation grant # 14-12-01227.

1. S. G. Davidson and M. Steslicka, *Basic Theory of Surface States*, Oxford Science, N.Y. (1996).
2. I. Tamm, Phys. Z. Sowjetunion **1**, 733 (1932).
3. A. A. Maradudin and G. Stegeman, in *Surface Phonons*, ed. by W. Kress and F. W. De Wette, Springer-Verlag, Berlin (1991), p. 5.
4. V. M. Agranovich and D. L. Mills, *Surface Polaritons*, North Holland, Amsterdam (1984).
5. P. Yeh, A. Yariv, and A. Y. Cho, Appl. Phys. Lett. **32**, 104 (1978).

6. Yu. S. Kivshar, Laser Phys. Lett. **5**, 703 (2008).
7. C. R. Rosberg, D. N. Neshev, W. Krolikowski, A. Mitchell, R. A. Vicencio, M. I. Molina, and Yu. S. Kivshar, Phys. Rev. Lett. **97**, 083901 (2006).
8. J. Du, S. Liu, Z. Lin, J. Zi, and S. T. Chui, Phys. Rev. A **83**, 035803 (2011).
9. R. S. Savelev, A. P. Slobozhanyuk, A. E. Miroshnichenko, Yu. S. Kivshar, and P. A. Belov, Phys. Rev. B **89**, 035435 (2014).
10. A. I. Kuznetsov, A. E. Miroshnichenko, Y. H. Fu, J. Zhang, and B. Lukyanchuk, Sci. Rep. **2**, 492 (2012).
11. A. B. Evlyukhin, S. M. Novikov, U. Zywietz, R. L. Eriksen, C. Reinhardt, S. I. Bozhevolnyi, and B. N. Chichkov, Nano Lett. **12**, 3749 (2012).
12. A. E. Krasnok, A. E. Miroshnichenko, P. A. Belov, and Yu. S. Kivshar, JETP Lett. **9**4, 593 (2011).
13. E. Palik, *Handbook of Optical Constants of Solids*, Academic Press, Boston (1985).
14. G. W. Mulholland, C. F. Bohren, and K. A. Fuller, Langmuir **10**, 2533 (1994).
15. R. A. Shore and A. D. Yaghjian, Radio Sci. **47**, RS2014 (2012).
16. W. H. Weber and G. W. Ford, Phys. Rev. B **70**, 125429 (2004).
17. J. Stratton, *Electromagnetic Theory*, McGraw-Hill, N.Y. (1941).